RSC Advances

ROYAL SOCIETY OF CHEMISTRY

www.rsc.org/advances

Journal Name RSCPublishing

ARTICLE

Aluminophosphate monoliths with high CO_2-over-N_2 selectivity and CO_2 capture capacity

Cite this: DOI: 10.1039/x0xx00000x

Received 00th January 2012,
Accepted 00th January 2012

DOI: 10.1039/x0xx00000x

www.rsc.org/

F. Akhtar,[*a,b] N. Keshavarzi,[a] D. Shakarova,[a] O. Cheung,[a,b] N. Hedin,[a,b] L. Bergström,[a]

Monoliths of microporous aluminophosphates ($AlPO_4$-17 and $AlPO_4$-53) were structured by binder-free pulsed current processing. Such monoliths could be important for carbon capture from flue gas. The $AlPO_4$-17 and $AlPO_4$-53 monoliths exhibited a tensile strength of 1.0 MPa and CO_2 adsorption capacity of 2.5 mmol/g and 1.6 mmol/g at 101 kPa at 0 °C, respectively. Analyses of single component CO_2 and N_2 adsorption data indicated that the $AlPO_4$-53 monoliths had an extraordinarily high CO_2-over-N_2 selectivity from binary gas mixture of 15 mol% CO_2 and 85 mol% N_2. The estimated CO_2 capture capacity of $AlPO_4$-17 and $AlPO_4$-53 monoliths in a typical pressure swing adsorption (PSA) process at 20 °C was higher than that of the commonly used zeolite 13X granules. Under cyclic sorption conditions, $AlPO_4$-17 and $AlPO_4$-53 monoliths were regenerated by lowering the pressure of CO_2. Regeneration was done without application of heat, which would regenerate them to their full capacity for CO_2 adsorption.

Introduction

Porous aluminophosphates ($AlPO_4$-n) are attractive materials for gas separation[1–3], adsorption[4], catalysis[5] and host-guest chemistry[6]. The 8-ring aluminophosphates exhibits crystalline micropores with pore windows that are similar to the kinetic diameter of light gas molecules. These aluminophosphates are therefore, of interest for CO_2, CH_4 and N_2 separation[2,3,7]. Liu et al.[3] have shown that the 8-ring aluminophosphates $AlPO_4$-17 and $AlPO_4$-53 offer high CO_2 capture capacities, high CO_2-over-N_2 selectivities and ease of regeneration. Deroche et al.[7] reported that $AlPO_4$-18 has a lower heat of CO_2 sorption than most zeolites. A low heat of CO_2 sorption would decreases the energy penalty associated with regeneration of the adsorbent to its full CO_2 adsorption capacity in a cyclic adsorption process.

Microporous powders are usually structured into granules and beads because beds of micron-sized powders exhibit very large pressure drops. A large pressure drop can result in clogs or blockages in some gas separation processes[8,9]. Typically, structured adsorbents are produced by shaping a mixture of the porous powder with an inorganic and organic binder into a body of the desired geometry[10-12]. The powder body is thermally treated to increase the mechanical strength. While aluminophosphates, silicoaluminophosphates and other ortho and pyro-phosphates powders have been processed to produce hierarchically porous catalytic supports with catalytic components, (e.g. Pt, Ag on zeolite Y, and zeolite ZK-5)[13-17], reports on structuring of $AlPO_4$-n powders to produce structured adsorbents are sparse.[18]

The efficiency of an adsorbent is decreased when the active component- the microporous powder- is diluted by a large proportion of an inert binder. Moreover, the inert binder is selectively removed in a chemically corrosive environment[19]. The selective removal of the binder can result in lowered mechanical stability of the structured adsorbent. The presence of the inert binder may also alter the adsorptive properties of the structured adsorbent.[8] Hence, there is a great interest in developing binder-less processing routes that can produce mechanically strong structured adsorbents with maximized volume efficiency. Previously, it was demonstrated in an elaborate, multi-step process, that clay and silica binders can be converted into active porous materials by hydrothermal treatment.[20-24] We developed a versatile pulsed current processing (PCP) route to directly produce mechanically strong, yet binder-free, hierarchically porous monoliths from e.g. microporous zeolite, mesoporous silica and macroporous diatomite powders[25-29].

In this work, we demonstrate that mechanically stable and binder-less structured adsorbents of $AlPO_4$-17 and $AlPO_4$-53 can be produced by PCP. With the optimized PCP temperature and pressure, the PCP-produced monoliths displayed a high CO_2 capture capacity and outstanding CO_2-over-N_2 selectivity. The CO_2 working capacity in a typical PSA process was evaluated and compared with commercial granules of zeolite 13X. Cyclic adsorption capacity and regeneration conditions to a full CO_2 adsorption capacity were determined for the $AlPO_4$-17 and $AlPO_4$-53 monoliths as well.

Experimental

Materials: The materials used were: aluminum iso-propoxide (98 wt%, Aldrich), ortho-phosphoric acid (85.0 wt% aqueous H3PO4, Aldrich), methylamine (Aldrich), N,N,N',N' tetramethyl-1,6- hexanediamine (TMHD, Aldrich) double deionized water (DDW), commercial 13X (Pingxiang Xintao Chemical Packaging Co. Ltd., China) beads of 1.5-2.5 mm in diameter.

Synthesis of $AlPO_4$ powders:

$AlPO_4$-17 synthesis: $AlPO_4$-17 was synthesized via hydrothermal synthesis. 3.42 g of aluminum iso-propoxide (98 wt%, Aldrich) was mixed in 9 cm3 of deionized water for 10 minutes. Thereafter 2.30 g of phosphoric acid (85 wt%, Aldrich) was added and the mixture was further agitated for 20 minutes. Then, 3.44 g of N,N,N',N' tetramethyl-1,6-hexanediamine (TMHD, Aldrich) was added to the mixture. The resulting gel was stirred for an additional 2 hours before it was transferred to Teflon lined stainless steel autoclave and heated to 200 °C for 9 h under static conditions.

$AlPO_4$-53 synthesis: $AlPO_4$-53 was synthesized using similar steps as $AlPO_4$-17. 3.13 g of aluminum iso-propoxide (98 wt%, Aldrich) was mixed in 21 cm3 of deionized water for 10 minutes. Thereafter 3.46 g of phosphoric acid (85 wt%, Aldrich) was added and the mixture was further agitated for 20 minutes. Then, 3.40 g of methylamine (Aldrich) was added to the mixture. The resulting gel was stirred for an additional 2 hours before it was transferred to Teflon lined stainless steel autoclave and heated to 150 °C for 168 h under static conditions. After hydrothermal synthesis, the AlPO4 products were separated from the reaction gel, washed with deionized water, and dried overnight at 100 °C. The organic structure direction agent (SDA) was removed by calcination. $AlPO_4$-17 was calcined at 600 °C (heating rate 10°C/min) for 6 hours under a slow flow of air. $AlPO_4$-53 was calcined at 400 °C (heating rate 10°C/min) for 48 hours under a slow flow of air.

Processing: Calcined $AlPO_4$-17 and $AlPO_4$-53 powders were consolidated into cylindrical monoliths in a graphite die of 12 mm in diameter by pulsed current processing (PCP) in a so-called spark plasma sintering equipment (Dr. Sinter 2050, Sumitomo Coal Mining Co., Ltd., Japan). Such consolidation was driven by electric heating in combination with compressive pressure. The powder assemblies were heated at a heating rate of 100 °C/min up to the target temperature, where the temperature was held for 3 minutes. A pressure of 20 MPa and 50 MPa was applied during heating and holding cycles. The temperature was measured using a K-type thermocouple. After the heating cycle, the die assemblies were cooled down to 100 °C before the ejection of consolidated monoliths from graphite dies.

Characterization: The microstructure of cylindrical monoliths was characterised with a field emission gun scanning electron microscope (FEG-SEM), JSM-7000F (JEOL, Tokyo, Japan) operating at an acceleration voltage of 5 kV. A small amount of each powder and a part of cleaved monolith were put on a double-sided carbon adhesive tape with the aluminum stub as the base for SEM. The crystal structure of as-synthesized powders and PCP consolidated monoliths were characterized by X-ray diffraction (XRD) on a PANalytical X'Pert PRO powder diffractometer (PANalytical, Almelo, Netherlands) (CuKα1 radiation λ=1.540598 Å) operating at 45 kV and 40 mA settings. XRD data was collected between 2θ =5.0–60.0°. The strength of the PCP consolidated monoliths of 12 mm in diameter and 8 mm in height was determined by diametral compression test by applying a displacement rate of 0.5 mm/min on a Zwick Z050 (Zwick GmBH Co & KG, Ulm, Germany) instrument. Mercury intrusion porosimetery was used to determine macropore volumes and pore size distributions for pores with diameters of 3 nm to 125 μm in PCP consolidated monoliths using an Auto Pore III 9410 (Micromeritics, Norcross GA, USA).

BET surface area and CO_2 and N_2 adsorption: Nitrogen adsorption-desorption experiments were performed at -196 °C on a Micrometrics ASAP2020 surface area analyzer (Micromeritics, Norcross GA, USA). The specimens were degassed at high vacuum (1×10^{-4} Pa) at 300 °C for 6 hours. The Brunauer-Emmet-Teller (BET) surface area was calculated using the nitrogen uptake of the specimen in the relative pressure range of 0.05-0.15 p/p_o. The CO_2 and N_2 adsorption measurements were performed on a Micrometrics Gemini V 2390 apparatus (Micromeritics, Norcross GA, USA) equipped with the room temperature add-on. CO_2 and N_2 adsorption measurements were recorded at 0 °C and 20 °C within a pressure range from 0 to 101 kPa. Isothermal conditions (± 0.1 °C) were maintained by a circulating bath (Huber Ministat 230) which contains a low molecular weight siloxane polymer. The temperature in the Dewar flask was measured by an external thermocouple and cross-calibrated to that of the circulating bath. Prior to adsorption measurements, the calcined $AlPO_4$-n powders and the consolidated monoliths were pre-treated under a flow of dry N_2 gas at a temperature of 300 °C for 8-10 h. The cyclic performance of the monoliths was tested by recording the CO_2 uptake of the samples after regeneration by only vacuum at room temperature.

Adsorption models and Ideal adsorbed solution theory (IAST): The traditional Langmuir isotherm model with two parameters was used to describe the adsorption isotherms of CO_2 and N_2. The traditional Langmuir isotherm model can be written as:[1]

$$q = \frac{q_m bP}{1 + bP} \quad (1)$$

where q and q_m are the uptake and the maximum uptake, respectively, b is equation constant and P is the equilibrium pressure. Langmuir model parameters were used as an input to the IAS theory to predict binary adsorption selectivity ($\alpha_{CO2/N2}$) from the single-component adsorption isotherms of CO_2 and N_2.

Results and Discussion

We previously studied binder-less consolidation of zeolites[26-28], mesoporous silica[29], and diatomite[25] by pulsed current processing (PCP) and showed that the porous particles could be consolidated into hierarchically porous monoliths without the

addition of binders. In this study, monoliths of $AlPO_4$-17 and $AlPO_4$-53 have been successfully consolidated using the same technique. We have found that a temperature of 650 °C and a compressive pressure of 20 MPa and 400 °C and 50 MPa is suitable for PCP of $AlPO_4$-17 powder ($AlPO_4$-17(p)) and for $AlPO_4$-53 powder ($AlPO_4$-53(p)), respectively, for producing mechanically stable monoliths with a high surface area. These consolidated $AlPO_4$-17 ($AlPO_4$-17mPCP650) and $AlPO_4$-53 ($AlPO_4$-53mPCP400) monoliths are relatively strong and display gas adsorption properties similar to the starting powders. Diametral compression tests of $AlPO_4$-17mPCP650 and $AlPO_4$-53mPCP400 have shown that the monoliths exhibit a tensile strength of 1.0 MPa (Table-1), comparable to zeolite monoliths prepared by PCP and colloidal processing[26,30,31].

The SEM micrographs of the monoliths (Fig. 1) show that the rod-like $AlPO_4$-17 and polyhedral $AlPO_4$-53 crystals have retained their well-defined and faceted morphologies after PCP. Fig. 1 display pores in-between the crystals in the PCP $AlPO_4$s. The median diameters of these macropores have been quantified by mercury intrusion porosimetry (Table 1), which show that the macropores are significantly larger in the $AlPO_4$-17 monolith when compared to the $AlPO_4$-53 monolith. Large macropores are advantageous as they limit the pressure drop over an adsorption column and enhance the mass transport of gas molecules[26,30,32].

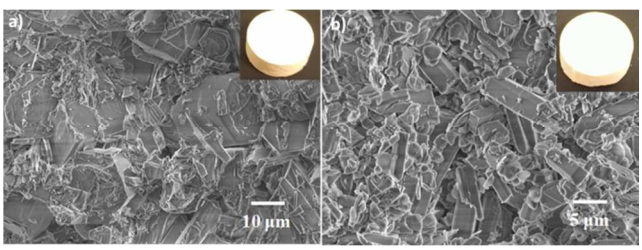

Figure 1. Scanning electron micrographs from fractured surfaces of: a) $AlPO_4$-17mPCP650; b) $AlPO_4$-53mPCP400. The insets show photographs of the monoliths.

Table 1. BET surface area, Langmuir surface area, macropore volume, macroporosity, median pore diameter and mechanical strength of monoliths prepared by pulsed current processing.

Monoliths	$AlPO_4$-17m PCP650	$AlPO_4$-53m PCP400
[a] S_{BET} (m²/g)	464	223
[b] $S_{Langmuir}$ (m²/g)	548	256
[c] $V_{Macropore}$ (cm^3/g)	0.26	0.32
[c] Macro-porosity (vol. %)	31.0	41.0
[c] Median pore diameter (µm)	3.50	0.70
Mechanical strength (MPa)	1.05±0.10	0.85±0.10

[a] BET surface area is calculated from N_2 adsorption data recorded at -196 °C; [b] Langmuir surface area is calculated from CO_2 adsorption data at 0 °C. [c] Macropore volume, macroporosity, and median pore diameter are determined by mercury intrusion porosimetry.

An optimum balance between adsorption activity, mass transfer and mechanical stability is required for gas separation by swing adsorption processes[8,33,35]. The combination of an optimized temperature and pressure during PCP has resulted in structured monoliths of $AlPO_4$-17 and $AlPO_4$-53 with a high CO_2 capture capacity and a relatively high mechanical strength (Table-1). The CO_2 and N_2 uptake on these monoliths of $AlPO_4$-17 and $AlPO_4$-53 (Fig. 2) show that the PCP temperature has significantly influenced the capacity for adsorption of CO_2.The $AlPO_4$-17 monoliths that have been treated by PCP at 650 °C have only a 12% reduced capacity as compared to the powder, Figure 2a-b. We ascribe this minor reduction in the CO_2 uptake to the bonding of $AlPO_4$-17 crystals at contact points. These contact points can alter the local microporous structure[27,28] during the PCP treatment by local amophization or phase transformation to a non-adsorbing phase. If the temperature during the PCP is higher than 650 °C, the capacities of the $AlPO_4$-17 monoliths are further reduced. $AlPO_4$-17 based monoliths that have been consolidated at 750 °C can only adsorb 1.2 mmol/g of CO_2. Similarly, the $AlPO_4$-53 monoliths that have been subjected to PCP at 400 °C and 50 MPa pressure also have only a slight decrease in the capacities to adsorb CO_2 and N_2, Figure 3c-d. The N_2 uptake on $AlPO_4$-17 and $AlPO_4$-53 powders and monoliths is small, as expected from the low electric quadrupole moment of N_2 (-4.6 x 10^{-40} Cm^{-2}) compared to CO_2 (-14 x 10^{-40} Cm^{-2})[36].

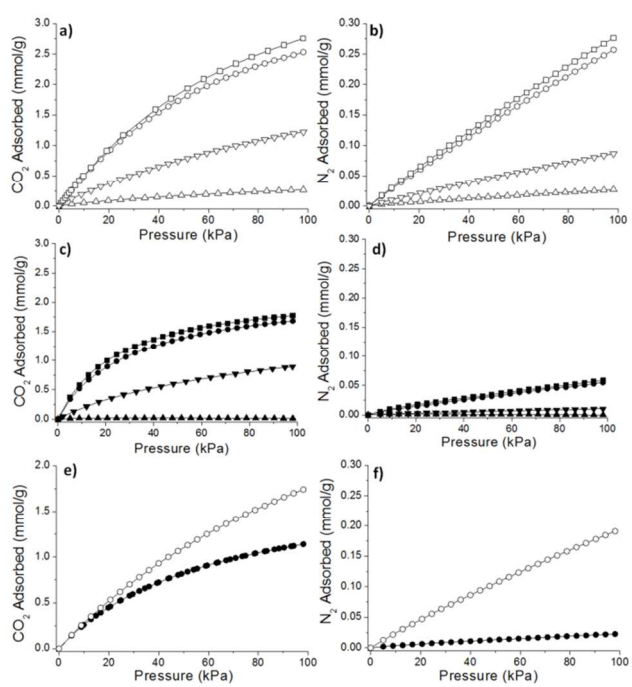

Figure 2. Adsorption isotherms of CO_2 and N_2 at 0 °C on powders and monoliths of $AlPO_4$-17 and $AlPO_4$-53 PCP consolidated at compressive pressure of 20 and 50 MPa, respectively; a) CO_2 uptake on $AlPO_4$-17: powder (□), monoliths prepared at 650 °C (○),750 °C (▽), and 950 °C (Δ); b) N_2 uptake on $AlPO_4$-17: powder (□), monoliths prepared at 650 °C (○),750 °C (▽), and 950 °C (Δ); c) CO_2 uptake on $AlPO_4$-53: powder (■), monoliths prepared at 400 °C (●),500 °C (▼),and 950 °C (▲); d) N_2 uptake on $AlPO_4$-53: powder (■), monoliths prepared at 400 °C (●), 500 °C (▼), and 950 °C (▲); e) CO_2 uptake at 20 °C on monoliths: $AlPO_4$-17-based prepared at 650 °C (○) and $AlPO_4$-53-based prepared at 400 °C (●); f) N_2 uptake at 20 °C on monoliths: $AlPO_4$-17-based prepared at 650 °C (○) and $AlPO_4$-53-based prepared at 400 °C (●).

When the $AlPO_4$-17(p) and $AlPO_4$-53(p) have been processed above the optimal temperature for PCP, the microporous powders transformed into a new dense $AlPO_4$ phase and a crystalline $AlPO_4$ phase, respectively (Fig. 3). These monoliths then have negligible capacities to adsorb CO_2 and N_2 (Fig. 3). Analyses of the XRD data (Fig. 3) show that $AlPO_4$-17 transforms into a sodalite $AlPO_4$ phase and that $AlPO_4$-53 transforms into tridymite $AlPO_4$ phase at 950 °C. It should be mentioned that although the sodalite structure is porous, the pore windows are too small for diffusion of CO_2 and N_2 molecules.

The CO_2 adsorption capacity at 0 °C of the $AlPO_4$-17mPCP650 is 2.5 mmol/g and 1.65 mmol/g for the $AlPO_4$-53mPCP400 at a partial pressure of 100 kPa (see Fig. 2). The N_2 adsorption is low on both monoliths, but is significantly lower on the $AlPO_4$-53mPCP400, 0.05 mmol/g (100 kPa) than that of the $AlPO_4$-17mPCP650, 0.24 mmol/g (100 kPa). The difference in CO_2 and N_2 adsorption capacity of $AlPO_4$-17mPCP650 and $AlPO_4$-53mPCP400 suggest that $AlPO_4$-17mPCP650 have high capacity for CO_2 adsorption and $AlPO_4$-53mPCP400 display an extraordinary high CO_2-over-N_2 selectivity.

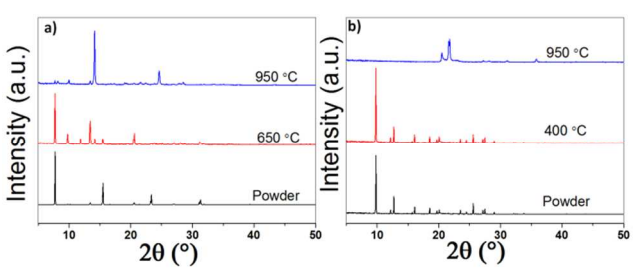

Figure 3. X-ray diffractograms of powders and monoliths of $AlPO_4$-17 (a) and $AlPO_4$-53 (b). The temperatures given in the figure represent the maximum temperature employed during pulsed current processing.

CO_2 selectivity is an important requirement for separation of CO_2 from flue gas. We can obtain a simple estimate of the CO_2-over-N_2 selectivity, $S_{CO2/N2}$, for a typical flue gas mixture that contains 15 mol % CO_2 and 85 mol % N_2 as the ratio of equilibrium mole fraction of CO_2 adsorbed at 15 kPa ($x_{CO_2}^{15}$) over the equilibrium mole fraction of N_2 adsorbed at 85 kPa ($y_{N_2}^{85}$), as follows

$$S_{CO_2/N_2} = \frac{x_{CO_2}^{15}.85}{y_{N_2}^{85}.15} \qquad (2)$$

The $S_{CO2/N2}$ at 20 °C is 17 for $AlPO_4$-17mPCP650 and 102 for $AlPO_4$-53mPCP400. The high CO_2-over-N_2 selectivity of $AlPO_4$ has been ascribed to kinetic or molecular sieving effects[3,37]. Molecular sieving or kinetic effects are related to the kinetic diameter of CO_2 (3.3Å) and N_2 (3.64Å) and the size of the 8 ring window of $AlPO_4$-17 and $AlPO_4$-53. $AlPO_4$-17 is a 8-ring aluminophosphate with a window size of 3.6 x 5.1 $Å^2$.[38] $AlPO_4$-53 is also a 8-ring aluminophosphate with a window size of 4.3 x 3.1 $Å^2$ along [100] direction[38], which is close to the kinetic diameter of CO_2 molecule. More physically correct estimates of the thermodynamic selectivity make use of ideal adsorbed solution (IAS) theory developed by Myers and Prausnitz[39-41]. It allows estimation of the co-adsorption equilibriums for CO_2 and N_2 mixtures from the single component isotherms of CO_2 and N_2. In IAST, Myers and Prausnitz[39] defined selectivity within a two phase model as the ratio of mole fraction of CO_2 in the adsorbed state (x_{CO_2}) over the mole fraction of CO_2 (y_{CO_2}) in the gas phase divided by the same relative fractions for N_2 (x_{N_2}, y_{N_2})

$$\alpha_{CO_2/N_2} = \frac{x_{CO_2}.y_{N_2}}{x_{N_2}.y_{CO_2}} \qquad (3)$$

Table 2. CO_2 and N_2 Henry's law constant and calculated CO_2-over-N_2 selectivity of monoliths prepared by pulsed current processing. The $AlPO_4$-17-based monolith was treated at 650 °C and the $AlPO_4$-53-based one at 400 °C.

Monoliths	Adsor-bate	[a]q_m (mmol/g)	[b] b (1/kPa)	K_H (qm x b) CO_2	K_H (qm x b) N_2	K_H CO_2/ K_H N_2	[c]Binary selectivity ($\alpha_{CO2/N2}$)
$AlPO_4$-17mPCP650	CO_2	4.389	0.0067	0.029	---	12.78	15
$AlPO_4$-17mPCP650	N_2	1.095	0.0021	---	0.0023		
$AlPO_4$-53mPCP400	CO_2	1.878	0.0157	0.0295	---	99.33	2800
$AlPO_4$-53mPCP400	N_2	0.0799	0.0039	---	0.0003		

[a],[b] Obtained from fitting adsorption isotherm at 293 K by Langmuir model. [c] Calculated by ideal adsorption solution theory at 100 kPa in CO_2 and N_2 binary mixture of composition 15 mol % CO_2 and 85 mol % N_2.

Table 2 shows that the binary CO_2-over-N_2 selectivity is very high for $AlPO_4$-53mPCP400. Hence, the favourable pore window dimensions of $AlPO_4$-53 are preserved after PCP and the monolith could selectively retard the diffusivity of N_2 and reduce its uptake kinetically or by molecular sieving[3,26,40,42]. The $AlPO_4$-17mPCP650 has high CO_2 uptake but the CO_2-over-N_2 selectivity is significantly smaller compared to $AlPO_4$-53mPCP400. CO_2 separation in industrial practice, e.g. flue gas scrubbing and natural or biogas upgrading, is considered economically feasible by adopting pressure swing adsorption (PSA) or vacuum swing adsorption process (VSA) at moderate temperatures, providing that the adsorbent has a low pressure drop, high working capacity and also small sensitivity to water adsorption[43-46]. In the interest of potentially using $AlPO_4$ monoliths in swing adsorption carbon capture processes (PSA or VSA), the amount of CO_2 that can be removed per kilogram of structured $AlPO_4$ monoliths needs to be determined. We have estimated the CO_2 capturing capacities in an idealized PSA process using the CO_2 adsorption isotherms in Fig. 2. The estimates in Fig. 4 assume that the flue gas from a small scale combustion plant contains 15 mol% CO_2 and 85 mol% N_2. The total pressure of the process is assumed to swing from 1 bar to 6 bar in a simple and hypothetical PSA process. The temperature of the flue gas is assumed to be 20 °C, this is mainly because CO_2 adsorption data are quite commonly reported at this temperature. We consider a small scale combustion plant only, as we doubt that it will be economic or technically possible to compress the full flue gas stack. In this gas mixture, the partial pressure of CO_2 at 1 bar and 6 bar in the flue gas corresponds to 0.15 bar and 0.90 bar, respectively. For these conditions, the CO_2 capture capacity can be defined as the difference between CO_2 uptake at 0.9 bar and 0.15 bar and represent the moles of CO_2 gas that can be removed in a PSA cycle per kilogram of the adsorbent.

Fig. 4a and b shows the CO_2 capture capacity of $AlPO_4$-17mPCP650 and $AlPO_4$-53mPCP400 in the highlighted region that corresponds to these PSA conditions, i.e. varying pressure from 1 bar to 6 bar. The CO_2 capture capacity of monoliths of $AlPO_4$-17mPCP650 is 1.4 mmol/g. The CO_2 capture capacity is comparable to that of several MOFs with large uptakes of CO_2, e.g. MOF 5[46], Mg-MOF-74[46], MOF-508[47] and higher compared to zeolite adsorbents[48,49] (Table 3).

Table 3. CO_2 capture capacity in a hypothetical pressure swing adsorption process at room temperature for MOFs and zeolite adsorbents in comparison with $AlPO_4$-17mPCP650 (current work).

Adsorbent (Monoliths/Powder	CO_2 adsorption capacity (mmol/g)
$AlPO_4$-17mPCP650	1.4
MOF-5	0.7
Mg-MOF-74	2.1
MOF-508	1.6
Silicalite	0.6
HZSM-5	1.0

The CO_2 capture capacity of monoliths of $AlPO_4$-53mPCP400 at 20 °C is 0.8 mmol/g. The CO_2 capture capacity is lower than $AlPO_4$-17mPCP650, however the CO_2 selectivity is higher on $AlPO_4$-53mPCP400. When compared with the CO_2 capture capacity of commercial granules of zeolite 13X, $AlPO_4$-17mPCP650 and $AlPO_4$-53mPCP400 display higher CO_2 capacities. Zeolite 13X is widely researched and accepted as a standard material with a potential use in CO_2 capture[30,31,50,51]. The CO_2 capture capacity of 13X granules is 0.7 mmol/g and 0.67 mmol/g in the first and second adsorption cycle, respectively. The total CO_2 adsorption capacity of 13X granules is reduced irreversibly after the first cycle from 2.9 to 2.5 mmol/g. This irreversible reduction is probably related to chemisorption of CO_2 on 13X granules as the reduced CO_2 capacity between the two cycles cannot be overcome without high temperature regeneration[50,51]. It should be noted that the flue gas contains water vapors which could reduce the CO_2 capture capacity of $AlPO_4$ monoliths and 13X granules further. However, it has been reported that aluminophosphates are less hydrophilic at lower partial pressure of water vapors[2,52]. Liu et al.[3] reported that the water adsorption capacity of $AlPO_4$-17, $AlPO_4$-53 and 13X powders was 0.17, 0.15 and 0.37 g/g, respectively. Zeolite

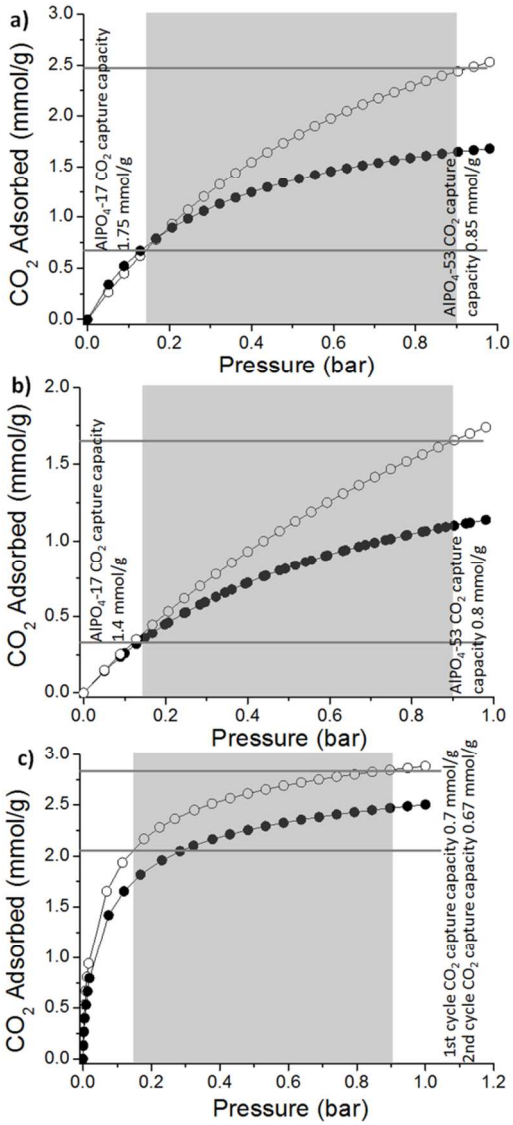

Figure 4. Determination of ideal working capacity of $AlPO_4$-17mPCP650, $AlPO_4$-53mPCP400, and commercial 13X granules in a hypothetical pressure swing adsorption (PSA) cycle. The working capacity in a PSA process is the difference in uptake between the high (6 bar) and low (1 bar) pressure extremes which correspond to 0.90 and 0.15 bar CO_2 pressure in flue gas containing 15 mol % CO_2 and 85 mol % N_2. a) CO_2 adsorption isotherm of $AlPO_4$-17mPCP650 (○) and $AlPO_4$-53mPCP400 (●) at 0 °C; b) CO_2 adsorption isotherm of $AlPO_4$-17mPCP650 (○) and $AlPO_4$-53mPCP400 (●) at 20 °C; c) CO_2 adsorption isotherm of 13X granules, first CO_2 adsorption cycle (○) and second CO_2 adsorption cycle (13X granules were regenerated by lowering the pressure (near vacuum conditions) without application of heat after first CO_2 adsorption cycle) (●). The shaded areas (in a,b and c) show the pressure swing cycle between 0.15 to 0.9 bar (corresponding to 1 bar and 6 bar pressure of flue gas containing 15 mol % CO_2 and 85 mol % N_2) and the parallel horizontal lines (in a,b and c) show the CO_2 working capacity of $AlPO_4$-17mPCP650, $AlPO_4$-53mPCP400 in a and b and 13X beads in c.

13X has a so-called type-1 water adsorption isotherm[53] and the $AlPO_4$-ns have so-called type-V water adsorption isotherms[52]. These shape differences implied that $AlPO_4$-17 and $AlPO_4$-53 not only adsorbed less water in the low pressure region compared to 13X zeolite, but that they are significantly less hydrophilic. Therefore, there will be no or only a slight reduction in the CO_2 capture capacity from (wet) flue gas. 13X granules show limited CO_2 capture capacity under PSA conditions (Fig. 4c) however they may be more useful materials in a VSA process where the pressure varies between 0.01 to 0.3 bar[48] for CO_2 capture from dry flue gas.

The cyclic adsorption performance of an adsorbent is an important property for its long term usage. Figure 5 shows that the CO_2 capture capacity of $AlPO_4$-17mPCP650 (Fig. 5a) and $AlPO_4$-53mPCP400 (Fig. 5b) monoliths do not show any significant changes over five adsorption cycles. The monoliths have been regenerated by lowering the pressure (near-vacuum conditions) and without applying heat. The unchanged CO_2 capture capacities are attributed to the absence of chemisorption on the less hydrophilic framework of $AlPO_4$-17 and $AlPO_4$-53 materials[3,52]. The cyclic adsorption performance of $AlPO_4$ monoliths is superior to zeolite 13X, which loses a fraction of its CO_2 adsorption capacity after first adsorption cycle (Fig. 4c). Typically, zeolites require heating to a high temperature for regeneration to their full CO_2 adsorption capacity[26,42,51]. Overall, the $AlPO_4$-17mPCP650 and $AlPO_4$-53mPCP400 show high mechanical stability, high CO_2 capture capacity in PSA, low hydrophilicity, cyclic performance and easy regeneration. These render them as potential materials with good CO_2 capture capacities, long life time and low cost for CO_2 capture from flue gas. They are in particular interesting for CO_2 removal processes that can tolerate a pressurization step.

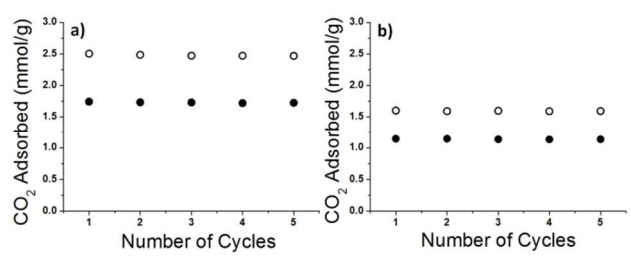

Figure 5. The cyclic CO_2 adsorption capacity of monoliths prepared by pulsed current processing at two temperatures 0 °C (○) and 20 °C (●). a) $AlPO_4$-17mPCP650, b) $AlPO_4$-53mPCP400. After each cycle, monoliths were regeneration only by lowering the pressure without application of heat.

Conclusions

Hierarchically porous and mechanically stable monoliths of $AlPO_4$-17 and $AlPO_4$-53 have been produced by pulse current processing (PCP) without adding any inorganic binders. The monoliths based on $AlPO_4$-17 show high CO_2 capture capacities and those based on $AlPO_4$-53 show very high CO_2-over-N_2 selectivities for a hypothetical flue gas mixture consisting of CO_2 and N_2. The estimated CO_2 capture capacities

of the $AlPO_4$-17 and $AlPO_4$-53 monoliths are superior to those of the standard zeolite 13X granules in a hypothetical PSA process. These monoliths display excellent cyclic performance and are also expected to be less affected by water than zeolite based monoliths. The low water sensitivity will reduce the cost for drying of the flue gas in an actual implementation of an adsorption driven capture of CO_2. Over all, the adsorptive properties, mechanical strength, CO_2 capture capacity and low energy cost for regeneration of aluminophosphate monoliths render them candidate structured adsorbents for CO_2 capture from pressurized flue gas mixtures.

Acknowledgements

This work has been financed by the Berzelii Center EXSELENT on Porous Materials. D. Shakarova acknowledges the Swedish Institute for the postdoctoral research fellowship.

Notes and references

[a]Department of Materials and Environmental Chemistry, Stockholm University, Stockholm 10691, Sweden
[b]Division of Materials Science, Luleå University of Technology, Luleå 97187, Sweden
[c]Berzelii Center EXSELENT on Porous Materials, Stockholm University, Stockholm 10691, Sweden
Corresponding author's Email: farid.akhtar@mmk.su.se and Ph. No. +46 8 163942

1 C. Martin, N. Tosi-Pellenq, J. Patarin, and J. Coulomb, Langmuir, 1998, 7463, 1774–1778.
2 M. L. Carreon, S. Li, and M. A. Carreon, Chem. Commun., 2012, **48**, 2310–2312.
3 Q. Liu, N. C. O. Cheung, A. E. Garcia-Bennett, and N. Hedin, ChemSusChem, 2011, **4**, 91–97.
4 L. Predescu, F. Tezel, and S. Chopra, Adsorption, 1997, **25**, 7–25.
5 G. J. Hutchings, I. D. Hudson, D. Bethell, and D. G. Timms, 1999, **299**, 291–299.
6 J. Yu and R. Xu, Chem. Soc. Rev., 2006, **35**, 593–604.
7 I. Deroche, L. Gaberova, and G. Maurin, Adsorption, 2008, **14**, 207–213.
8 F. Rezaei and P. A. Webley, Sep. Purif. Technol., 2010, **70**, 243–256.
9 F. Rezaei and P. A. Webley, Chem. Eng. Sci., 2012, **69**, 270–278.
10 C. N. Satterfield, Heterogeneous catalysts in industrial practice, Krieger Publishing Company New York, 1996.
11 Y. Y. Li, S. P. Perera, B. D. Crittenden, and J. Bridgwater, Powder Technol., 2001, **116**, 85–96.
12 F. Akhtar, L. Andersson, S. Ogunwumi, N. Hedin, and L. Bergström, J. Eur. Ceram. Soc., 2014, **34**,1643-1666.
13 Y. Arita, 2009, P2009–57305A Japan.
14 Q. Chang, H. He, J. Zhao, M. Yang, and J. Qu, Environ. Sci. Technol., 2008, **42**, 1699–1704.
15 M. Machida, K. Murakami, S. Hinokuma, K. Uemura, K. Ikeue, M. Matsuda, M. Chai, Y. Nakahara, and T. Sato, Chem. Mater., 2009, **21**, 1796–1798.
16 P. Meriaudeau, V. A. Tuan, L. N. Hung, Zeolites 1997, **19**, 449-451.
17 T. Degnan, S. McCullen, K. D. Schmitt, H. Hatzikos, US Pat. 5185310, 1993.
18 W. Li, Y. Zhu, X. Guo, K. Nakanishi, K. Kanamori, and H. Yang, Sci. Technol. Adv. Mater., 2013, 14, 045007.
19 N. Keshavarzi, F. Akhtar, and L. Bergström, J. Mater. Res., 2013, **28**, 2253–2259.
20 M. L. Pavlov, O. S. Travkina, R. A. Basimova, I. N. Pavlova, and B. I. Kutepov, Pet. Chem., 2009, **49**, 36–41.
21 M. Pavlov, R. Basimova, and O. Travkina, Oil gas Bus., 2012, 459–469.
22 S. Kulprathipanja, US Pat. 4248737, 1981.
23 M. Rauscher, T. Selvam, W. Schwieger, and D. Freude, Microporous Mesoporous Mater., 2004, **75**, 195–202.
24 F. Scheffler, W. Schwieger, D. Freude, H. Liu, W. Heyer, and F. Janowski, Microporous Mesoporous Mater., 2002, **55**, 181–191.
25 F. Akhtar, P. O. Vasiliev, and L. Bergström, J. Am. Ceram. Soc., 2009, **92**, 338–343.
26 F. Akhtar, Q. Liu, N. Hedin, and L. Bergström, Energy Environ. Sci., 2012, **5**, 7664.
27 F. Akhtar, A. Ojuva, S. K. Wirawan, J. Hedlund, and L. Bergström, J. Mater. Chem., 2011, **21**, 8822.
28 P. O. Vasiliev, F. Akhtar, J. Grins, J. Mouzon, C. Andersson, J. Hedlund, and L. Bergström, ACS Appl. Mater. Interfaces, 2010, **2**, 732–737.
29 P. O. Vasiliev, Z. Shen, R. P. Hodgkins, and L. Bergström, Chem. Mater., 2006, **18**, 4933–4938.
30 A. Ojuva, F. Akhtar, A. P. Tomsia, and L. Bergström, ACS Appl. Mater. Interfaces, 2013, **5**, 2669–76.
31 F. Akhtar and L. Bergström, J. Am. Ceram. Soc., 2011, **94**, 92–98.
32 F. Rezaei, A. Mosca, P. A. Webley, J. Hedlund and P. Xiao, Ind. Eng. Chem. Res. 2010, **49**, 4832–4841.
33 F. Rezaei and P. A. Webley, Chem. Eng. Sci., 2009, **64**, 5182–5191.
34 A. Mosca, J. Hedlund, P. A. Webley, M. Grahn, and F. Rezaei, Microporous Mesoporous Mater., 2010, **130**, 38–48.
35 F. Rezaei and M. Grahn, Ind. Eng. Chem. Res., 2012, **51**, 4025–4034.
36 C. Graham, D. A. Imrie, and R. E. Raab, Mol. Phys., 1998, **93**, 49–56.
37 O. Cheung, Q. Liu, Z. Bacsik, and N. Hedin, Microporous Mesoporous Mater., 2012, **156**, 90–96.
38 Database of Zeolite Structures, http://www.iza-structure.org/databases/
39 A. L. Myers and J. M. Prausnitz, AIChE J., 1965, **11**, 121–127.
40 R. T. Yang, Gas separation by adsorption processes, London: Imperial College Press, London, UK, 1997.
41 D. Do Duong, Adsorption Analysis: Equilibria and Kinetics, Imperial College Press, 1998.
42 Q. Liu, A. Mace, Z. Bacsik, J. Sun, A. Laaksonen, and N. Hedin, Chem. Commun., 2010, **46**, 4502–4504.
43 R. P. Lively, R. R. Chance, and W. J. Koros, Ind. Eng. Chem. Res., 2010, **49**, 7550–7562.
44 M. Ho, G. Allinson, and D. Wiley, Ind. Eng. Chem. Res., 2008, **47**, 4883–4890.
45 G. D. Pirngruber and D. Leinekugel-le-cocq, Ind. Eng. Chem. Res., 2013, **52**, 5985-5996.
46 J. M. Simmons, H. Wu, W. Zhou, and T. Yildirim, Energy Environ. Sci., 2011, **4**, 2177–2185.
47 L. Bastin, P. S. Barcia, E. J. Hurtado, J. A. C. Silva, A. E. Rodrigues, and B. Chen, J. Phys. Chem. C, 2008, **112**, 1575–1581.
48 S. K. Wirawan and D. Creaser, Microporous Mesoporous Mater., 2006, **91**, 196–205.
49 P. Xiao, J. Zhang, P. Webley, G. Li, R. Singh, and R. Todd, Adsorption, 2008, **14**, 575–582.
50 N. Konduru, P. Lindner, and N. M. Assaf-Anid, AIChE J., 2007, **53**, 3137–3143.
51 F. Akhtar, L. Andersson, N. Keshavarzi, and L. Bergström, Appl. Energy, 2012, **97**, 289–296.
52 B. Newalkar, R. Jasra, V. Kamath, and S. Bhat, Microporous Mesoporous Mater., 1998, 129-137.
53 J. Kim, C. Lee, W. Kim, and J. Lee, J. Chem. Eng. Data, 2003, 137–141.